PCCP

Stability of polycyclic aromatic hydrocarbons on graphite: Resistance to horizontal displacement

Journal:	*Physical Chemistry Chemical Physics*
Manuscript ID	CP-ART-02-2025-000567.R1
Article Type:	Paper
Date Submitted by the Author:	13-Mar-2025
Complete List of Authors:	Kikkawa, Yoshihiro; National Institute of Advanced Industrial Science and Technology (AIST), Tsuzuki, Seiji; The University of Tokyo, Applied Physics; Yokohama National University, Institute of Advanced Sciences

ARTICLE

Stability of polycyclic aromatic hydrocarbons on graphite: Resistance to horizontal displacement

Received 00th January 20xx,
Accepted 00th January 20xx

DOI: 10.1039/x0xx00000x

Yoshihiro Kikkawa[a]* and Seiji Tsuzuki[b]*

The stability of adsorbed molecules on surfaces depends on the magnitude of adsorbate–substrate interaction energies and the resistance of these molecules to horizontal displacement. Therefore, it is essential to analyse both interaction energy (E_{int}) and its change with horizontal displacement (ΔE_{int}). In physisorbed monolayers at a highly oriented pyrolytic graphite (HOPG)/solvent interface, molecular building blocks often contain both aromatic and alkyl chain moieties, as aromatic molecules without additional substituents are difficult to observe via scanning tunnelling microscopy. This suggests that aromatic molecules have less adsorption stability on the HOPG than *n*-alkanes, though the underlying reason remains unclear. In this study, we performed dispersion-corrected density functional theory calculations to evaluate E_{int} and ΔE_{int} of polycyclic aromatic hydrocarbons (PAHs) on a graphite model surface ($C_{96}H_{24}$). ΔE_{int} was analysed for benzene, naphthalene, and anthracene. The maximum ΔE_{int} ($\Delta E_{int(max)}$) is related to the barrier height for lateral migration. The $\Delta E_{int(max)}$ per N_c showed directional dependence and ranged from 0.015 to 0.20 kcal mol^{-1}, with the largest value for PAHs being about two-thirds that of *n*-alkanes (0.30 kcal mol^{-1}), indicating greater mobility of the former. These findings demonstrate that aromatic and alkyl chain moieties in two-dimensional assemblies exhibit distinct resistance against horizontal migration. The preferential role of alkyl chains suggests that molecular assemblies align with the graphite lattice, prioritising alkyl unit positioning over aromatic orientation.

Introduction

Molecular self-assembly has been harnessed to create intriguing nanostructures with remarkable properties, often comparable to or surpassing those in nature.[1] Noncovalent interactions play a crucial role in forming ordered molecular assemblies, which can be achieved through the rational design and synthesis of molecular building blocks.[1] Supramolecular interactions include dispersion forces, metal coordination, hydrogen bonding, and halogen bonding. In two-dimensional assemblies on surfaces, characteristic molecular arrangements in chemisorbed and physisorbed monolayers have been visualised using scanning tunnelling microscopy (STM).[2]

Physisorbed monolayers have been particularly prepared at the highly oriented pyrolytic graphite (HOPG)/solvent interface, where molecules with specific shapes and interaction sites facilitate the formation of diverse two-dimensional assemblies.[3] Most molecules utilised in such assemblies contain both an aromatic core and alkyl chain units. These units interact not only with each other (intermolecular interactions) but also with the HOPG surface (molecule–substrate interactions) to form well-organised two-dimensional structures. The flat-on orientation of alkyl chains (where the symmetry plane of the alkyl chain is parallel to the HOPG plane) is preferred over the edge-on orientation (where the symmetry plane is perpendicular) as it aligns with the lattice direction of HOPG.[4]

The intermolecular interaction of *n*-alkanes on graphite surfaces has been investigated using experimental techniques such as temperature-programmed desorption (TPD) measurements[5] and theoretical approaches such as density functional theory (DFT), second-order Møller–Plesset perturbation theory (MP2), force field calculations, and molecular dynamics simulations.[6] In our previous study,[6f] we performed dispersion-corrected DFT calculations to examine the intermolecular interactions and stability of *n*-alkanes on $C_{54}H_{18}$ and $C_{96}H_{24}$ as graphite model surfaces. The interaction energies of *n*-alkanes on $C_{54}H_{18}$ increased with the number of carbon atoms in alkyl chains, consistent with the TPD results reported by Tait et al.[5d] The increase in interaction energy per carbon atom was approximately −1.9 kcal mol^{-1}. Dispersion forces primarily contributed to the attractive interactions between *n*-alkanes and the graphite model surface.

The π-stacked structure of polycyclic aromatic hydrocarbons (PAHs) has been observed in natural and artificial systems,[7] with dispersion forces identified as the primary attractive force.[8] π–π stacking plays a crucial role in stabilising the layered structure of graphite, whose interlayer cohesion energies (E_{coh}) have been investigated using experimental[9] and theoretical methods.[10] The reported E_{coh} per carbon atom is summarised in Table S1. Experimental methods for determining E_{coh} include the characterisation of collapsed carbon nanotubes using transmission electron microscopy (TEM), cleavage energy measurements of

[a] National Institute of Advanced Industrial Science and Technology (AIST), Tsukuba Central 5, 1-1-1 Higashi, Tsukuba, Ibaraki 305-8565, Japan
E-mail: y.kikkawa@aist.go.jp
[b] Department of Applied Physics, The university of Tokyo, Tokyo 113-8656, Japan
E-mail: tsuzuki.seiji@mail.u-tokyo.ac.jp.

Supplementary Information available: Optimised geometry of benzene-pyrene complex; Interaction energy potentials of flat-on and edge-on oriented benzene on $C_{96}H_{24}$; E_{int} and intermolecular distance of PAHs on $C_{96}H_{24}$; Interlayer cohesion energies reported in previous reports; E_{int} and ΔE_{int} values obtained by different calculation methods; ΔE_{int} change associated with the rotation of PAHs; Comparison of E_{int} between PAHs and *n*-alkanes on $C_{96}H_{24}$. See DOI: 10.1039/x0xx00000x

graphite layers via atomic force microscopy, and desorption energy measurements of PAHs from HOPG using TPD.[9] The reported E_{coh} per carbon atom ranged from 0.81 to 1.20 kcal mol^{-1}. Theoretical calculations using van der Waals density functional theory (vdW-DFT) and dispersion-corrected DFT estimated E_{coh} values between 1.11 and 1.22 kcal mol^{-1}.[10] The E_{coh} per carbon atom obtained from theoretical calculations closely aligns with the values determined through experimental methods.

In two-dimensional assemblies of alkylated aromatic molecules on HOPG, the aromatic units within the molecular building blocks interact with the HOPG surface via π–π interactions, alongside interactions involving alkyl chains. Numerous STM studies have demonstrated that alkyl chain moieties preferentially align along the HOPG lattice direction, whereas aromatic moieties exhibit relatively low orientational sensitivity to the HOPG surface.[2,3] Furthermore, the two-dimensional assemblies of aromatic molecules without alkyl chain moieties are difficult to observe using STM at the solid/liquid interface. This suggests that aromatic and alkyl chain moieties possess distinct adsorption stability characteristics. However, the fundamental mechanisms underlying these differences remain unclear. The magnitude of adsorption energies and the stability of the adsorbed molecules against horizontal displacement on the graphite surface are key factors influencing the stability and persistence of physisorbed two-dimensional assemblies. However, to the best of our knowledge, the stability of aromatic molecules and their resistance to horizontal displacement on graphite surfaces have not been systematically investigated.

In this study, we performed dispersion-corrected DFT calculations to evaluate the interaction energies (E_{int}) of PAHs with graphite model surfaces ($C_{54}H_{18}$ and $C_{96}H_{24}$) and the changes in these interaction energies (ΔE_{int}) with horizontal displacement. The validity of the calculated E_{int} values was confirmed by comparing them with previously reported values from TPD measurements.[9b,9e] Dispersion-corrected DFT and MP2 calculations were performed to verify the accuracy of the ΔE_{int} values. We then evaluated the ΔE_{int} values of benzene, naphthalene, and anthracene to assess the effect of the carbon number (N_c) in PAHs on resistance to horizontal displacement. Additionally, we compared the ΔE_{int} values of PAHs and *n*-alkanes to explore their distinct characteristics in the stable formation of two-dimensional assemblies.

Computational details

DFT and *ab initio* calculations were performed using the Gaussian 16 software (Gaussian, Wallingford, CT, USA).[11] The geometries of isolated molecules and complexes were optimised at the B3LYP/6-31G* level[12] with Grimme's D3 dispersion correction[13] (B3LYP-D3/6-31G*). The optimised structures of isolated $C_{54}H_{18}$ and $C_{96}H_{24}$ were used to prepare the initial configurations for the geometry optimisations of the $C_{54}H_{18}$–PAHs and $C_{96}H_{24}$–PAHs complexes. During these geometry optimisations, the geometries of $C_{54}H_{18}$ and $C_{96}H_{24}$ were fixed. The E_{int} values for the complexes were calculated at the B3LYP-D3/6-311G** level unless otherwise specified. Basis set superposition error (BSSE)[14] was corrected using the counterpoise method.[15] The CCSD(T) level E_{int} at the basis set limit was estimated based on MP2-level E_{int} at the basis set limit, combined with CCSD(T)-level E_{int} calculations using the 6-311G** basis set. The MP2-level E_{int} at the basis set limit was determined from MP2 calculations using the aug-cc-pVDZ and aug-cc-pVTZ basis sets. Details of this estimation method have been previously reported.[4c]

Since the optimised structures of the $C_{96}H_{24}$–PAHs complexes formed approximately AB-stacked configurations, the E_{int} values for the complexes were calculated while horizontally displacing the PAHs from the AB-stacking position. The distance between the PAHs and the π plane of $C_{54}H_{18}$ or $C_{96}H_{24}$ was fixed at 3.40 Å, corresponding to the equilibrium distance in the optimised complexes. The change in E_{int} associated with horizontal displacement (ΔE_{int}) was calculated using the equation[6f]

$$\Delta E_{int} = E_{int} - E_{int}(0),$$

where $E_{int}(0)$ is the E_{int} calculated at the position of AB-stacking structure.

Results and discussion

Verification of B3LYP-D3 level interaction energies for PAHs on a graphite model surface.

To confirm the accuracy of the B3LYP-D3/6-311G** level interaction energies, the E_{int} value for the benzene–pyrene complex obtained at this level was compared with the estimated CCSD(T) level E_{int} at the basis set limit, as CCSD(T) level E_{int} values at the basis set limit are generally close to experimental interaction energies in the gas phase.[16] The optimised geometry of the benzene–pyrene complex is shown in Fig. S1. The E_{int} value for the complex at the B3LYP-D3/6-311G** level was –5.75 kcal mol^{-1}, while the CCSD(T) level E_{int} value at the basis set limit was –6.20 kcal mol^{-1}. The difference (approximately 7.2**%**) is relatively small, indicating that B3LYP-D3/6-311G** level calculations are sufficiently accurate for determining the E_{int} values of PAH stacks.

To further verify the B3LYP-D3/6-311G** level interaction energies, the E_{int} values of the $C_{96}H_{24}$–PAH complexes were calculated. The optimised geometries of these complexes are shown in Fig. 1(a-k). The number of carbon atoms (N_c) in PAHs ranges from 6 to 42. In the optimised geometries, all π-planes of PAHs are parallel to the π-plane of $C_{96}H_{24}$, exhibiting AB-type stacking. Previous studies[10] and our calculations in Fig. S2 confirm that AB-type stacking structures are the most stable. The mean distances of the PAH carbon atoms from the π-plane of $C_{96}H_{24}$ and their corresponding E_{int} values are presented in Table S2. The absolute E_{int} values ($|E_{int}|$) of the complexes were plotted as a function of *N*c in the PAHs (Fig. 1(l)). The $|E_{int}|$ increased linearly, and the plots closely overlapped with the

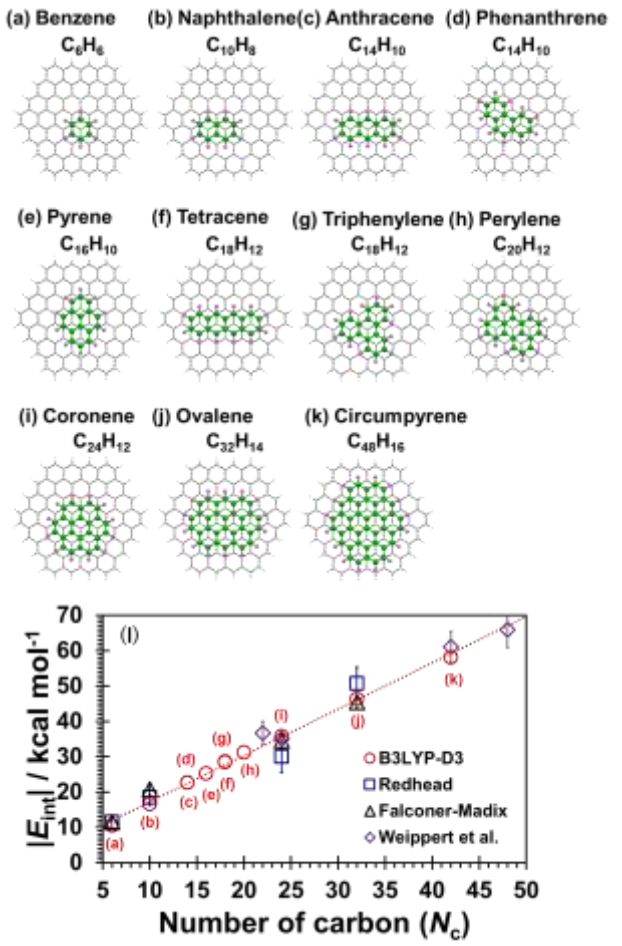

Fig. 1 (a-k) Optimised geometries of $C_{96}H_{24}$ complexes with PAHs. (l) Plots of $|E_{int}|$ for $C_{96}H_{24}$–PAH complexes as a function of the number of carbon atoms in the PAHs (N_c): Red circles are plots of $|E_{int}|$ obtained at the B3LYP-D3/6-311G** level, and their linear regression equation (red dotted line) is $|E_{int}| = 1.31N_c + 4.14$ (R^2 = 0.997); blue squares and black triangles are derived from the TPD experiments by Zacharia et al. with different analyses.[9b] The linear regression equation by Readhead analysis (blue square) is $|E_{int}| = 1.37N_c + 2.92$ (R^2 = 0.941), while that by Falconer-Madix analysis (black triangle) is $|E_{int}| = 1.22N_c + 6.03$ (R^2 = 0.984); purple rhombi are plots of TPD-derived $|E_{int}|$ by Weippert et al.[9e], and the linear regression equation is $|E_{int}| = 1.31N_c + 5.09$ (R^2 = 0.997) : kcal mol^{-1}.

experimental E_{int} values obtained from TPD measurements,[9b,9e] as shown in Fig. 1(l). The slope of these plots represents the $|E_{int}|$ per N_c in the PAHs. The slope obtained in this study (1.31 kcal mol^{-1}) is comparable to the experimentally determined values (1.22–1.37 kcal mol^{-1}).

Björk *et al.*[10d] proposed that the E_{int} values of the PAHs are the sum of the interaction energies of graphene-like carbon (E_{cc}) and benzene-like carbon (E_{CH}) and can be expressed as follows:

$$|E_{int}| = N_cE_{CC} + N_H(E_{CH} - E_{CC})$$

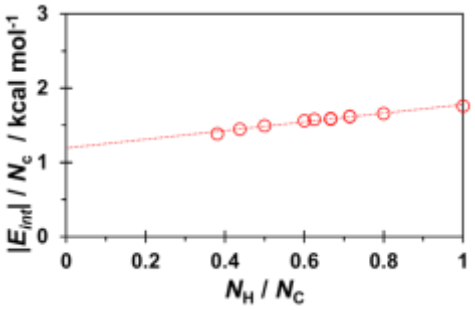

Fig. 2 $|E_{int}|/N_c$ vs N_H/N_C plots for the $C_{96}H_{24}$ complexes with PAHs, where N_C and N_H are the number of C and H atoms in PAHs, respectively. The linear regression equation (red dotted line) is $|E_{int}|/N_c = 0.58\ N_H/N_C + 1.19$ (R^2 = 0.977) : kcal mol^{-1}.

where N_C and N_H represent the number of carbon and hydrogen atoms in the PAHs, respectively. In PAHs, graphene-like carbon atoms are covalently bonded to three adjacent carbon atoms, while benzene-like carbon atoms are bonded to two carbon atoms and one hydrogen atom. The $|E_{int}|/N_c$ versus N_H/N_c plots yield the E_{CC} value as the intercept, which corresponds to the graphite interlayer cohesion energy per carbon atom.[9e,10d] To perform the same analysis, we plotted $|E_{int}|/N_c$ as a function of N_H/N_c, as shown in Fig. 2. The calculated E_{CC} is 1.19 kcal mol^{-1}, which is consistent with previously reported cohesion energies obtained from both experimental methods[9] and theoretical calculations,[10] as summarised in Table S1. These results indicate that the B3LYP-D3 calculations employed in this study are reliable for analysing the intermolecular interaction energies (E_{int}) between PAHs and $C_{96}H_{24}$.

Accuracy of B3LYP-D3 level interaction energies with respect to horizontal displacement

The ΔE_{int} values associated with the horizontal displacement of benzene in the $C_{54}H_{18}$–benzene complex along the *y*-axis from the AB-stacking position was calculated because AB-type stacking structure is most stable (Fig. S2).[10] First, the basis set dependence in the B3LYP-D3 calculations was examined using the 6-31G*, 6-311G* and 6-311G** basis sets. The E_{int} and ΔE_{int} values, along with their plots as a function of the horizontal displacement (*d*), are presented in Table S3 and Fig. S3, respectively. The ΔE_{int} values obtained using B3LYP-D3/6-311G** were nearly identical to those using B3LYP-D3/6-31G* and B3LYP-D3/6-311G*, indicating minimal basis set effects.

The ΔE_{int} values of the $C_{54}H_{18}$–benzene complex calculated using B3LYP-D3 were compared with those obtained using MP2 and dispersion-corrected double-hybrid DFT calculations (B2PLYP and mPW2PLYP).[17] The calculated E_{int} and ΔE_{int} values are summarised in Table S4. The ΔE_{int} plots obtained using all calculation methods overlapped closely, as shown in Fig. S4. Additionally, DFT calculations using the BLYP[18] and PBE[19] functionals with D3 dispersion corrections yielded similar ΔE_{int} values (Table S5 and Fig. S5). These results

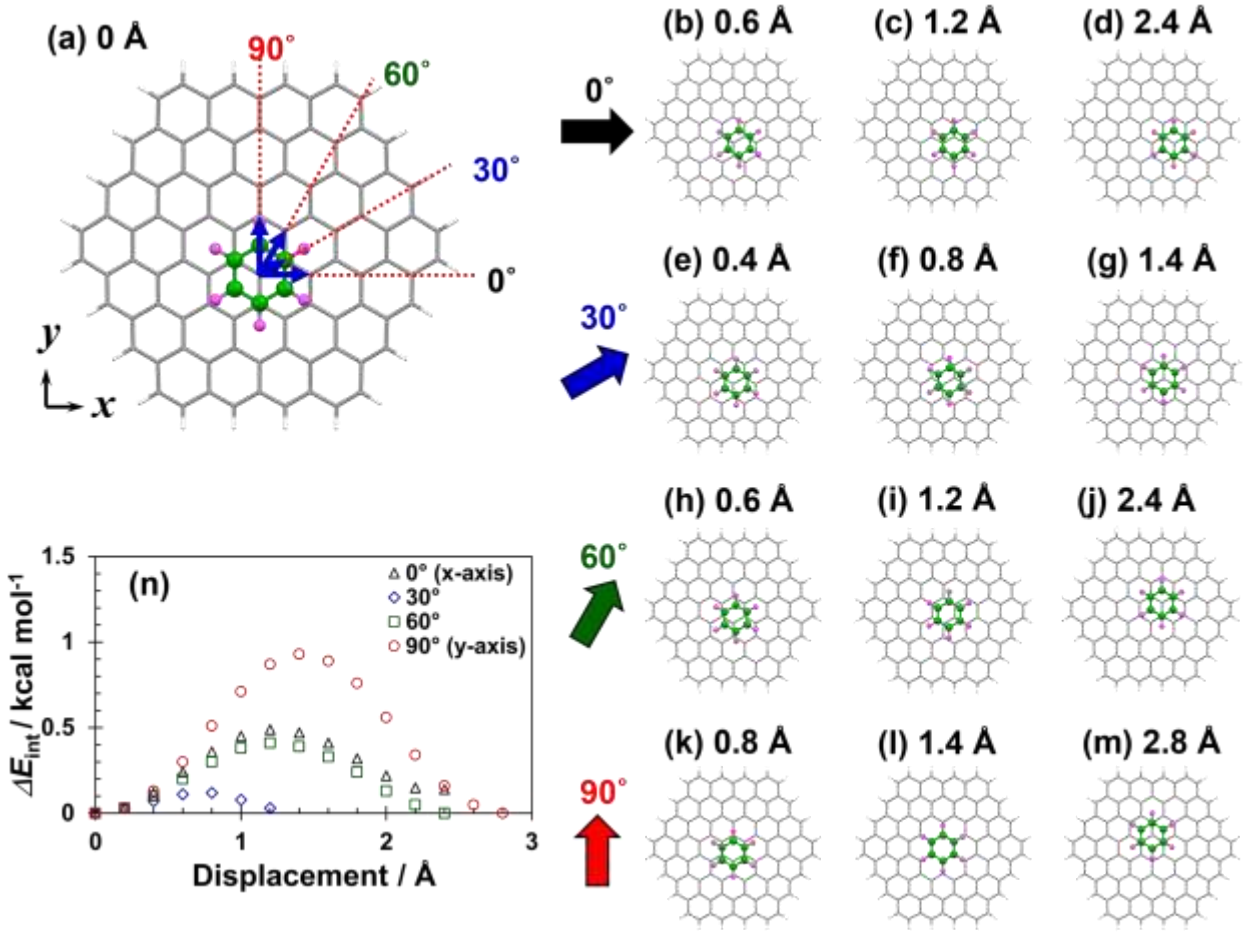

Fig. 3 Horizontal displacement of benzene in $C_{96}H_{24}$–benzene complex and plots of ΔE_{int} associated with the horizontal displacement: (a) The AB-stacking structure (initial position) of the complex and the four directions of displacement of benzene; benzene was moved horizontally along the directions that resulted in angles of 0˚ (b-d), 30˚ (e-g), 60˚ (h-j), and 90˚ (k-m) with the *x*-axis. (n) Plots of ΔE_{int} for the complex calculated at the B3LYP-D3/6-311G** level associated with horizontal displacement of benzene. Black triangles, blue rhombi, green squares, and red circles correspond to ΔE_{int} associated with horizontal displacements along the directions that result in angles of 0˚, 30˚, 60˚ and 90˚ with the *x*-axis.

indicate that the choice of the calculation method has minimal impact on ΔE_{int}, confirming that the B3LYP-D3/6-311G** calculations are reliable for analysing ΔE_{int} associated with the horizontal displacement of PAHs in the complexes. Therefore, subsequent E_{int} and ΔE_{int} calculations associated with horizontal displacement were performed at the B3LYP-D3/6-311G** level.

Change in interaction energy between benzene and $C_{96}H_{24}$ associated with horizontal displacement

The E_{int} value for the $C_{96}H_{24}$–benzene complex was calculated by horizontally displacing benzene from AB-stacking position while maintaining a fixed distance of 3.4 Å between benzene and $C_{96}H_{24}$. The position of benzene was varied horizontally in increments of 0.2 Å along four different directions at 30˚ intervals (Fig. 3(a-m)), corresponding to angles of 0˚, 30˚, 60˚, and 90˚ with respect to the *x*-axis. The calculated E_{int} and ΔE_{int} values are listed in Table S6, and ΔE_{int} is plotted as a function of the horizontal displacement (*d*) in Fig. 3(n). When benzene moves at an angle of 30˚, its centre follows a C-C bond of $C_{96}H_{24}$. In this case, ΔE_{int} increases, reaching a maximum at *d* = 0.8 Å. However, even this maximum value ($\Delta E_{int(max)}$) is relatively small (0.12 kcal mol^{-1}). In contrast, when benzene moves at an angle of 90˚, ΔE_{int} reaches a maximum ($\Delta E_{int(max)}$ = 0.93 kcal mol^{-1}) at *d* = 1.4 Å and is approximately 7.8 times larger than the $\Delta E_{int(max)}$ value along 30˚. At this maximum (*d* = 1.4 Å), the projected positions of the six carbon atoms in benzene completely overlap with those of $C_{96}H_{24}$. As benzene continues moving at an angle of 90˚, ΔE_{int} decreases to zero at *d* = 2.8 Å. For displacements along 0˚ and 60˚, the $\Delta E_{int(max)}$ values are moderate, measuring 0.49 and 0.41 kcal mol^{-1}, respectively. These results indicate that the magnitude of ΔE_{int} associated with horizontal displacement varies significantly depending on the direction of benzene movement. Furthermore, differences in $\Delta E_{int(max)}$ appear to arise from the degree of overlap between the carbon atoms of benzene and those of $C_{96}H_{24}$.

Origin of ΔE_{int} associated with horizontal displacement

The ΔE_{int} plots associated with the horizontal displacement of benzene along the *y*-axis, calculated for the $C_{54}H_{18}$–benzene complex using the Hartree-Fock method (Table S7 and Fig. S6), exhibit a trend similar to that observed at the MP2 level. This similarity suggests that dispersion interactions have a negligible effect on ΔE_{int}. Instead, the primary cause of ΔE_{int} variations associated with horizontal displacement is short-range interactions, specifically the exchange repulsion resulting from the overlap between the carbon atoms of benzene and those of $C_{54}H_{18}$.

Effect of the number of carbon atoms PAHs on ΔE_{int} associated with horizontal displacement.

We extended the analysis of ΔE_{int} associated with the horizontal displacement from benzene to PAHs (naphthalene and anthracene). The four displacement directions for naphthalene and anthracene are illustrated in Figs. S7 and S8. The E_{int} and ΔE_{int} values calculated for the $C_{96}H_{24}$ complexes of naphthalene and anthracene, associated with horizontal displacement, are summarised in Tables S8 and S9. The ΔE_{int} plots for the $C_{96}H_{24}$ complexes of naphthalene and anthracene are compared with those for the $C_{96}H_{24}$–benzene complex in Fig. 4. Regardless of the displacement direction, $\Delta E_{int(max)}$ increases with N_c. Additionally, naphthalene and anthracene exhibit a strong directional dependence in ΔE_{int} associated with horizontal displacement, similar to benzene. Specifically, $\Delta E_{int(max)}$ is the smallest and largest when displacement occurs along 30° and 90°, respectively, while intermediate values are observed along 0° and 60°. For displacement along 30°, the $\Delta E_{int(max)}$ values for benzene, naphthalene, and anthracene are 0.12, 0.19, and 0.24 kcal mol^{-1}, respectively. For displacement along 90°, the $\Delta E_{int(max)}$ values are significantly larger: 0.93, 1.60, and 2.14 kcal mol^{-1}, respectively. These differences in $\Delta E_{int(max)}$, depending on the movement direction of aromatic molecules, arise from the varying degrees of overlap between the carbon atoms of the PAHs and those of $C_{96}H_{24}$ during displacement. The extremely small $\Delta E_{int(max)}$ when aromatic molecules move along 30° suggests that an aromatic molecule adsorbed on graphite can migrate easily in this specific direction while remaining adsorbed.

The dependence of $\Delta E_{int(max)}$ on the direction of movement and N_c can be more clearly analysed using the $\Delta E_{int(max)}$ versus N_c plot (Fig. 5). The $\Delta E_{int(max)}$) value per *N*c is smallest (0.015 kcal mol^{-1}) when displacement occurs along 30° direction, while the $\Delta E_{int(max)}$ values are 2.9, 4.6, and 10.1 times larger for displacements along 0°, 60°, and 90°, respectively. For the displacement along 90°, the analysis of $\Delta E_{int(max)}$ plots was extended to PAHs with larger N_c, and we investigated whether the molecular shape affects the $\Delta E_{int(max)}$ or not. As shown in Fig. S9, PAHs with the same N_c but different molecular

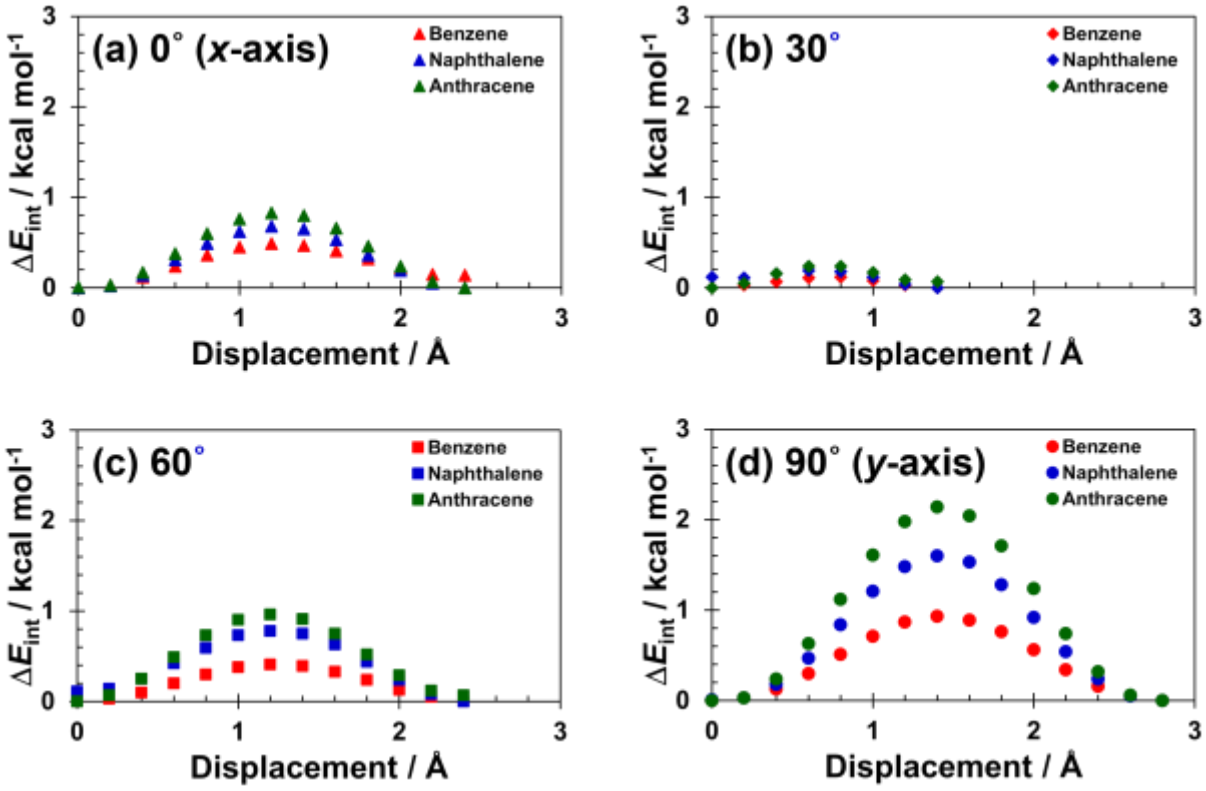

Fig. 4 Plots of B3LYP-D3/6-311G** level ΔE_{int} associated with horizontal displacement for the $C_{96}H_{24}$ complexes with benzene, naphthalene, and anthracene along four directions resulting in angles of (*a*) 0°, (b) 30°, (c) 60° and (d) 90° with the *x*-axis: Red, blue, and green symbols indicate ΔE_{int} calculated for benzene, naphthalene and anthracene complexes, respectively.

shapes (such as anthracene and phenanthrene; tetracene and triphenylene) showed no significant difference in the $\Delta E_{int(max)}$ values. In addition, both linear and non-linear shaped PAHs provided nearly the same $\Delta E_{int(max)}$ per N_c (0.20 kcal mol^{-1}). This suggests that $\Delta E_{int(max)}$ increases in proportion to N_c with little dependence on the shape of PAHs. As reported in our previous study,[6f] $\Delta E_{int(max)}$ for the horizontal displacement of *n*-alkanes on $C_{96}H_{24}$ also exhibits N_c dependence. The value of $\Delta E_{int(max)}$ per N_c for *n*-alkanes undergoing horizontal displacement was approximately 0.30 kcal mol^{-1}. This value is nearly 20 times larger than the $\Delta E_{int(max)}$ value per N_c for PAHs moving along 30˚ (0.015 kcal mol^{-1}), where $\Delta E_{int(max)}$ is the smallest. It is also two-thirds as large as the $\Delta E_{int(max)}$ per N_c for the PAHs moving along 90˚ (0.20 kcal mol^{-1}), where $\Delta E_{int(max)}$ is the largest. Since the $\Delta E_{int(max)}$ values are expected to correlate with the barrier heights for horizontal displacement of adsorbed molecules,[6f] the extremely small value of $\Delta E_{int(max)}$ per N_c for the PAHs along 30˚, compared with that for *n*-alkanes, suggests that PAHs can change their position on graphite surfaces more easily than *n*-alkanes at the same N_c.

Change in interaction energy associated with rotation

The change in ΔE_{int} for the $C_{96}H_{24}$–benzene complex associated with the rotation of benzene around its C_6 symmetry axis at the AB-stacking position is minimal, measuring less than 0.07 kcal mol^{-1} (Table S10 and Fig. S10). Similarly, for the rotation of naphthalene and anthracene in the $C_{96}H_{24}$ complexes, ΔE_{int} remains below 0.8 kcal mol^{-1}. The magnitude of ΔE_{int} variations with rotation appears to be related to the degree of overlap between the carbon atoms of PAHs and $C_{96}H_{24}$. Even for large N_c values, the $\Delta E_{int(max)}$ associated with rotation is significantly smaller than those observed for horizontal displacement.

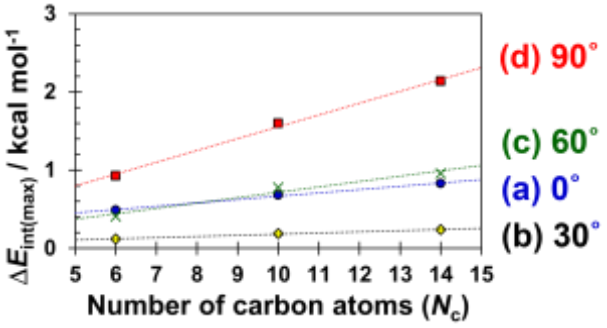

Fig. 5 Plots of $\Delta E_{int(max)}$ (maximum ΔE_{int} associated with horizontal displacement) at the B3LYP-D3/6-311G** level as a function of N_c: (a) $\Delta E_{int(max)}$ associated with displacement in the 0˚ direction (Fig. 4a) (blue circles), the linear regression equation is $\Delta E_{int(max)} = 0.043N_c + 0.242$ ($R^2 = 0.995$); (b) $\Delta E_{int(max)}$ associated with displacement in the 30˚. (Fig. 4b) (yellow rhombi), the linear regression equation is $\Delta E_{int(max)} = 0.015N_c + 0.033$ ($R^2 = 0.991$); (c) $\Delta E_{int(max)}$ associated with displacement in the 60˚. (Fig. 4c) (green cross marks), the linear regression equation is $\Delta E_{int(max)} = 0.069N + 0.029$ ($R^2 = 0.962$); (d) $\Delta E_{int(max)}$) associated with displacement in the 90˚ direction (Fig. 4d) (red squares), the linear regression equation is $\Delta E_{int(max)} = 0.151N + 0.044$ ($R^2 = 0.996$): kcal mol^{-1}.

Further comparison between PAHs and *n*-alkanes

Not only PAHs have smaller $\Delta E_{int(max)}$ values associated with horizontal displacement than *n*-alkanes of the same carbon number, but they also exhibit lower $|E_{int}|$ values than their corresponding *n*-alkanes, as shown in Tables S2, S11 and Fig. S11. Although a linear increase in $|E_{int}|$ accompanied with N_c is observed for both PAHs and *n*-alkanes, the increase in $|E_{int}|$ per N_c for PAHs (1.37 kcal mo^{l-1}) is approximately 70% of that for *n*-alkanes (1.96 kcal mo^{l-1}). The interaction energy potentials for the $C_{96}H_{24}$ complexes with benzene, naphthalene, *n*-hexane, and *n*-decane were calculated by varying their distances from the π-plane of $C_{96}H_{24}$ (Fig. S12). The distances at the potential minima for the PAH complexes (benzene and naphthalene) are 3.4 Å, while for the *n*-alkane complexes (*n*-hexane and *n*-decane), the minima occur at 3.5 Å. When the distance exceeds the equilibrium value, E_{int} becomes less negative than that of their corresponding *n*-alkanes with the same N_c. Previous studies have reported that dispersion interactions are the primary source of attraction in π-stacks of aromatic molecules[8] and in *n*-alkane interactions with a graphite model surface.[4c] These results suggest that dispersion interactions between *n*-alkane and $C_{96}H_{24}$ are stronger than those between the corresponding PAHs and $C_{96}H_{24}$. This difference is likely due to the orientation of hydrogen atoms bonded to carbon atoms. In PAHs, the π-planes of PAHs and $C_{96}H_{24}$ are parallel, and the C–H bonds in PAHs are also parallel to the π-plane of $C_{96}H_{24}$. In contrast, in *n*-alkanes, one of the two methylene hydrogen atoms points diagonally toward the π-plane of $C_{96}H_{24}$. This difference between the hydrogen atom orientation in PAHs and *n*-alkanes likely influences the strength of the dispersion interactions with $C_{96}H_{24}$.

Thus, we quantitatively revealed the differences between E_{int} and ΔE_{int} of PAHs and *n*-alkanes against horizontal displacement. In two-dimensional assemblies, the aromatic core and alkyl chain moieties of molecular building blocks exhibit distinct characteristics in terms of adsorption energy and resistance to horizontal displacement. Although both aromatic and alkyl chain units contribute to adsorption on graphite, as discussed above, the adsorption energy and barrier height for horizontal displacement are greater for alkyl chains than for aromatic units. These findings suggest that alkyl chain units play a dominant role over aromatic units in determining the molecular orientation within two-dimensional assemblies. In other words, molecules preferentially organise themselves in configurations that maintain the relative positions of the alkyl chain units with respect to the underlying graphite lattice, even at the expense of the orientation of the aromatic units.

Conclusions

Both intermolecular interaction energy (E_{int}) and its variation with the horizontal displacement (ΔE_{int}) of PAHs on a graphite model surface ($C_{96}H_{24}$) were evaluated using dispersion-corrected DFT calculations. Benzene, naphthalene, and anthracene were selected to examine the effect of the number of carbon atoms (N_c) on ΔE_{int}. The magnitude of ΔE_{int} depended on the direction of horizontal displacement: the maximum ΔE_{int} ($\Delta E_{int(max)}$) was the smallest and largest along 30° and 90°, respectively. Furthermore, $\Delta E_{int(max)}$ increased with increasing N_c in PAHs. When PAHs were displaced along 90°, the value of $\Delta E_{int(max)}$ per N_c (0.20 kcal mol^{-1}) was two-thirds that of *n*-alkanes (0.30 kcal mol^{-1}), suggesting that the barrier height for the horizontal displacement of PAHs is lower than that of *n*-alkanes. Additionally, the $|E_{int}|$ values of PAHs with $C_{96}H_{24}$ were smaller than those of *n*-alkanes at the same N_c. These findings indicate that PAHs exhibit lower adsorption stability and greater mobility on graphite than *n*-alkanes. As a result, the aromatic moieties in molecules forming two-dimensional assemblies are less constrained by the position and orientation of the graphite lattice compared to alkyl chain units.

We demonstrated that estimations of E_{int} and ΔE_{int} provide valuable insights into the stability of molecules in two-dimensional assemblies on a graphite surface. These findings are expected to contribute to advancing surface molecular self-assemblies with potential applications in coatings, lubrication, friction reduction, and molecular devices.

Author contributions

Yoshihiro Kikkawa: Conceptualisation, Methodology, Data curation, Formal analysis, Investigation, Visualisation, Writing – original draft, Writing – review & editing. Seiji Tsuzuki: Conceptualisation, Methodology, Data curation, Formal analysis, Investigation, Visualisation, Writing – original draft, Writing – review & editing.

Conflicts of interest

There are no conflicts to declare.

Data availability

The data supporting this article have been included as part of the Supplementary Information.

Acknowledgements

This work was partially supported by a JSPS KAKENHI grant (JP23H01702) to Y. K. and JST CREST grant (JPMJCR18J2) to S.T.

References

1 For examples: (a) D. Pochan and O. Scherman, *Chem. Rev.*, 2021, **121**, 13699; (b) K. Ariga, *Bull. Chem. Soc. Jpn,* 2024, **97**, uoad001; (c) P. K. Hashim, J. Bergueiro, E. W. Meijer and T. Aida, *Prog. Polym. Sci.*, 2020, **105**, 101250; (d) C. Kahlfuss, J. A. Wytko and J. Weiss, *ChemPlusChem*, 2017, **82**, 584–594. (e) V. Benekou, A. Candini, A. Liscio and V. Palermo, *ChemPlusChem*, 2024, **89**, e202400133; (f) Y. Li, D. Liang, R. Wang, S. Yang, W. Liu, Q. Sang, J. Pu, Y. Wang and K. Qian, *Small*, 2024, **20**, 2405318.

2 For examples: (a) R. K. Smith, P. A. Lewis and P. S. Weiss, *Prog. Surf. Sci.*, 2004, **75**, 1–68; 15; (b) S. De Feyter and F. C. De Schryver, *J. Phys. Chem. B*, 2005, **109**, 4290; (c) S. Uemura, R. Tanoue, N. Yilmaz, A. Ohira and M. Kunitake, *Materials (Basel)*, 2010, **3**, 4252; (d) D. B. Amabilino, *Supramolecular Chemistry at Surfaces*, Royal Society of Chemistry, London, 2016.

3 For examples: (a) J. A. A. W. Elemans, *Adv. Funct. Mater.*, 2016, **26**, 8932. (b) J. Teyssandier, K. S. Mali and S. De Feyter, *ChemistryOpen*, 2020, **9**, 225; (c) L. Verstraete and S. De Feyter, *Chem. Soc. Rev.,* 2021, **50**, 5884. (d) S. Liu, Y. Norikane and Y. Kikkawa, *Beilstein J. Nanotechnol.*, 2023, **14**, 872.

4 (a) B. Ilan, G. M. Florio, M. S. Hybertsen, B. J. Berne and G. W. Flynn, *Nano Lett.*, 2008, **8**, 3160; (b) T. Yang, S. Berber, J. F. Liu, G. P. Miller and D. Tománek, *J. Chem. Phys.*, 2008, **128**, 124709; (c) Y. Kikkawa and S. Tsuzuki, *Phys. Chem. Chem. Phys.*, 2023, **25**, 11331.

5 (a) K. R. Paserba and A. J. Gellman, *Phys. Rev. Lett.*, 2001, **86**, 4338; (b) K. R. Paserba and A. J. Gellman, *J. Chem. Phys.*, 2001, **115**, 6737; (c) A. J. Gellman and K. R. Paserba, *J. Phys. Chem. B*, 2002, **106**, 13231; (d) S. L. Tait, Z. Dohnálek, C.T. Campbell and B. D. Kay, *J. Chem. Phys.*, 2006, **125**, 234308.

6 (a) C. Thierfelder, M. Witte, S. Blankenburg, E. Rauls and W. G. Schmidt, *Surf. Sci.*, 2011, **605**, 746; (b) E. Londero, E. K. Karlson, M. Landahl, D. Ostrovskii, J. D. Rydberg and E. Schröder, *J. Phys. Condens. Matter*, 2012, **24**, 424212; (c) K. Kamiya and S. Okada, *Jpn. J. Appl. Phys.*, 2013, **52**, 04CN07; (d) S. Conti and M. Cecchini, *J. Phys. Chem. C*, 2015, **119**, 1867–1879; (e) L. Verstraete, T. Rinkovec, H. Cao, H. I. Reeves, J. N. Harvey and S. De Feyter, *J. Phys. Chem. C*, 2021, **125**, 1557; (f) Y. Kikkawa and S. Tsuzuki, *Phys. Chem. Chem. Phys.*, 2024, **26**, 24314.

7 For examples: (a) R. Thakuria, N. K. Nath and B. K. Saha, *Cryst. Growth Des.*, 2019, **19**, 523; (b) E. A. Meyer, R. K. Castellano and F. Diederich, *Angew. Chem. Int. Ed.,* 2003, **42**, 1210; (c) S. Grimme, *Angew. Chem., Int. Ed.*, 2008, **47**, 3430;(d) T. Chen, M. Li and J. Liu, *Cryst. Growth Des.,* 2018, **18**, 2765.

8 (a)S. Tsuzuki, K. Honda, T. Uchimaru, M. Mikami and K. Tanabe, *J. Am. Chem. Soc.*, 2002, **124**, 104; (b) S. Tsuzuki, K. Honda, T. Uchimaru and M. Mikami, *J. Chem. Phys.*, 2004, **120**, 647; (c) C. D. Sherrill, *Acc. Chem. Res.*, 2013, **46**, 1020.

9 (a) L. X. Benedict, N. G. Chopra, M. L. Cohen, A. Zettl, S. G. Louie and V. H. Crespi, *Chem. Phys. Lett.*, 1998, **286**, 490; (b) R. Zacharia, H. Ulbricht and T. Hertel, *Phys. Rev. B*, 2004, **69**, 155406; (c) E. Koren, E. Lörtscher, C. Rawlings, A. W. Knoll and U. Duerig, *Science*, 2015, **348**, 679; (d) J. Wang, D. C. Sorescu, S. Jeon, A. Belianinov, S. V. Kalinin, A. P. Baddorf and P. Maksymovych, *Nat. Commun.*, 2016, **7**, 13263; (e) J. Weippert, J. Hauns, J. Bachmann, A. Böttcher, X. Yao, B. Yang, A. Narita, K. Müllen and M. M. Kappes, *J. Chem. Phys.*, 2018, **149**, 194701.

10 (a) S. D. Chakarova-Käck, E. Schröder, B. I. Lundqvist and D. C. Langreth, *Phys. Rev. B*, 2006, **96**, 146107; (b) E. Ziambaras, J. Kleis, E. Schröder and P. Hyldgaard, *Phys. Rev. B*, 2007, **76**,

155425; (c) S. Lebègue, J. Harl, T. Gould, J. G. Ángyán, G. Kresse and J. F. Dobson, *Phys. Rev. Lett.,* 2010, **105**, 196401; (d) J. Björk, F. Hanke, C.-A. Palma, P. Samori, M. Cecchini and M. Persson, *J. Phys. Chem. Lett.,* 2010, **1**, 3407-3412; (e) A. Ambrosetti, A. M. Reilly, R. A. DiStasio, Jr. and A. Tkatchenko, *J. Chem. Phys.*, 2014, **140**, 18A508.

11 M. J. Frisch, G. W. Trucks, H. B. Schlegel, G. E. Scuseria, M. A. Robb, J. R. Cheeseman, G. Scalmani, V. Barone, G. A. Petersson, H. Nakatsuji, X. Li, M. Caricato, A. V. Marenich, J. Bloino, B. G. Janesko, R. Gomperts, B. Mennucci, H. P. Hratchian, J. V. Ortiz, A. F. Izmaylov, J. L. Sonnenberg, D. Williams-Young, F. Ding, F. Lipparini, F. Egidi, J. Goings, B. Peng, A. Petrone, T. Henderson, D. Ranasinghe, V. G. Zakrzewski, J. Gao, N. Rega, G. Zheng, W. Liang, M. Hada, M. Ehara, K. Toyota, R. Fukuda, J. Hasegawa, M. Ishida, T. Nakajima, Y. Honda, O. Kitao, H. Nakai, T. Vreven, K. Throssell, J. A. Montgomery, Jr., J. E. Peralta, F. Ogliaro, M. J. Bearpark, J. J. Heyd, E. N. Brothers, K. N. Kudin, V. N. Staroverov, T. A. Keith, R. Kobayashi, J. Normand, K. Raghavachari, A. P. Rendell, J. C. Burant, S. S. Iyengar, J. Tomasi, M. Cossi, J. M. Millam, M. Klene, C. Adamo, R. Cammi, J. W. Ochterski, R. L. Martin, K. Morokuma, O. Farkas, J. B. Foresman and D. J. Fox, *Gaussian 16, Revision* C.01, Gaussian, Inc., Wallingford, CT, 2016.

12 A. D. Becke, *J. Chem. Phys.*, 1993, **98**, 5648.

13 S. Grimme, J. Antony, S. Ehrlich and H. Krieg, *J. Chem. Phys.*, 2010, **132**, 154104.

14 B. J. Ransil, *J. Chem. Phys.*, 1961, **34**, 2109.

15 S. F. Boys and F. Bernardi, *Mol. Phys.*, 1970, **19**, 553.

16 T. H. Dunning, Jr., *J. Phys. Chem. A*, 2000, **104**, 9062.

17 L. Goerigk and Stefan Grimme, *J. Chem. Theory Comput.,* 2011, **7**, 291.

18 (a) A. D. Becke, *Phys. Rev. A: At., Mol., Opt. Phys.*, 1988, **38**, 3098; (b) C. Lee, W. Yang and R. G. *Parr, Phys. Rev. B: Condens. Matter Mater. Phys.*, 1988, **37**, 785.

19 J. P. Perdew, K. Burke and M. Ernzerhof, *Phys. Rev. Lett.*, 1996, **77**, 3865.

The data supporting this article have been included as part of the Supplementary Information.